Solar Phys (2014) 289:2459–2471
DOI 10.1007/s11207-014-0491-0

The Evolution of the Net Twist Current and the Net Shear Current in Active Region NOAA 10930

Yogita Suthar · P. Venkatakrishnan · B. Ravindra · S.N.A. Jaaffrey

Received: 3 July 2013 / Accepted: 3 February 2014 / Published online: 5 March 2014

Abstract The electric current exists because of the non-potential magnetic field in solar active regions. We present the evolution of net current in the solar active region NOAA 10930 as the sum of shear current and twist current by using 27 high-resolution vector magnetograms obtained with *Hinode*/SOT-SP during 9 – 15 December 2006. This active region was highly eruptive and produced a large number of flares ranging from B to X class. We derived local distribution of shear and twist current densities in this active region and studied the evolution of net shear current (NSC) and net twist current (NTC) in the N-polarity and S-polarity regions separately. We found the following: i) The twist current density was dominant in the umbrae. ii) The footpoint of the emerging flux rope showed a dominant twist current. iii) The shear current density and twist current density appeared in alternate bands around the umbrae. iv) On the scale of the active region, NTC was always larger than NSC. v) Both NTC and NSC decreased after the onset of an X3.4 class flare that occurred on 13 December 2006.

Keywords Sun: electric current · Sun: magnetic fields · Sun: sunspots

Y. Suthar (✉) · S.N.A. Jaaffrey
Department of Physics, University College of Science, Mohanlal Sukhadia University, Udaipur 313 001, India
e-mail: pushpayogita@gmail.com

S.N.A. Jaaffrey
e-mail: Jaaffrey@gmail.com

P. Venkatakrishnan
Udaipur Solar Observatory, Physical Research Laboratory, P.O. Box 198, Dewali, Badi Road, Udaipur 313 001, India
e-mail: pvk@prl.res.in

B. Ravindra
Indian Institute of Astrophysics, Koramangala, Bangalore 560 034, India
e-mail: ravindra@iiap.res.in

1. Introduction

The non-potential magnetic field manifests as the electric currents in solar active regions (ARs). The distribution of the vertical current density in active regions inferred from vector magnetic fields has been investigated by several authors (Moreton and Severny, 1968; Krall *et al.*, 1982; Ding *et al.*, 1987; Lin and Gaizauskas, 1987; Abramenko, Gopasiuk, and Ogir', 1991; Hofmann and Kalman, 1991; Chen and Zhang, 1992; Wang *et al.*, 1996). All these studies are concerned with the relationship between the distribution of electric currents and solar flares. The non-potentiality relates to the existence of electric currents that can trigger solar flares (Lin and Gaizauskas, 1987). The evolution of an electric current system may originate from two possibilities: one is the emergence of a new electric current system from below the photosphere (Leka *et al.*, 1996), and the second is the rearrangement of the magnetic field in the solar photosphere (Zhang, 1995). Parker (1996) argued that the values of vertical current densities inferred from vector magnetograms are severely affected by the spatial resolution of the magnetograph. Wang *et al.* (1996) examined the temporal variation of the total vertical current in an active region and suggested that the existence of strong current system contributes to flare activity. The shear and twist components of the vertical currents provide basic information on the total current (Zhang, 2001; Leka and Barnes, 2003). Zhang (2010) analyzed individual magnetic fibrils in the solar active region NOAA 10930 on 12 December 2006. He studied magnetic fibril fields and the relationship between the shear and twist components of the electric current around the magnetic inversion line. He found that the individual magnetic fibrils were dominated by the shear component and the large-scale magnetic region was dominated by the twist component of the electric current. However, a study of net current in AR 10930 by Ravindra *et al.* (2011) showed that the net current changed with time during flux emergence. In this paper our objective is to examine the evolution of the net shear current (NSC) and net twist current (NTC) separately in the positive (N) and negative (S) polarity regions in AR 10930 during 9 – 15 December 2006.

In Section 2, we divide the electric current density into twist and shear components. In Section 3, we describe the data; in Section 4 we present our results. Finally in Section 5 we provide the discussion of our results along with the conclusions.

2. Electric Current Density in AR 10930

The study of photospheric electric current in active regions is important because of its relation to the non-potential magnetic field. The electric current cannot be measured directly in the solar atmosphere. The current can be only derived indirectly from measurements of the vector magnetic field $\boldsymbol{B}$. The plasma distorts the magnetic field and the curl of this magnetic field produces a current according to Ampere's law (Parker, 1979). The electric current density is

$$\boldsymbol{J} = \frac{1}{\mu_0}(\nabla \times \boldsymbol{B}), \tag{1}$$

where $\mu_0 = 4\pi \times 10^{-3}\ \mathrm{G\,m\,A^{-1}}$ (G: gauss) is the permeability in free space and the unit of $\boldsymbol{J}$ is $\mathrm{A\,m^{-2}}$. We divided the electric current density into two components, as has been done in Zhang (2001),

$$\boldsymbol{J} = \frac{1}{\mu_0}(\nabla B) \times \boldsymbol{b} + \frac{B}{\mu_0}\nabla \times \boldsymbol{b}, \tag{2}$$

where $\boldsymbol{B} = B\boldsymbol{b}$ and $\boldsymbol{b}$ is the unit vector along the direction of the magnetic field and $B = \sqrt{(B_x^2 + B_y^2 + B_z^2)}$. The first term in Equation (2) is caused by the inhomogeneity of the magnetic field, and the second term is caused by the twist in the magnetic field. Thus, we wish to examine the role of both magnetic gradient and magnetic twist in the evolution of an active region. From Equation (2), the z-component of the electric current density can be written in the form

$$J_z = \frac{1}{\mu_0}\left(b_y \frac{\partial B}{\partial x} - b_x \frac{\partial B}{\partial y}\right) + \frac{B}{\mu_0}\left(\frac{\partial b_y}{\partial x} - \frac{\partial b_x}{\partial y}\right), \tag{3}$$

where b_x and b_y are the x- and y-components of $\boldsymbol{b}$, and the first and second terms are shear and twist components of the electric current density, respectively. Their area integration gives the net shear current (NSC) and the net twist current (NTC).

For comparing the contributions of shear and twist components to the vertical current density, we used the following ratios defined by

$$R_1 = \frac{|((\nabla B) \times \boldsymbol{b})_z|}{|((\nabla B) \times \boldsymbol{b})_z| + |(B(\nabla \times \boldsymbol{b}))_z|}, \tag{4}$$

$$R_2 = \frac{|(B(\nabla \times \boldsymbol{b}))_z|}{|((\nabla B) \times \boldsymbol{b})_z| + |(B(\nabla \times \boldsymbol{b}))_z|}. \tag{5}$$

The derivative of $\boldsymbol{B}$ in the z-direction is omitted because it is not available by observations currently.

3. Description of Data

We used the vector magnetograms of NOAA 10930 observed on 9 – 15 December 2006 with the Spectro-Polarimeter of *Solar Optical Telescope* (SOT-SP; Tsuneta *et al.*, 2008; Shimizu *et al.*, 2008; Suematsu *et al.*, 2008; Ichimoto *et al.*, 2008) onboard the *Hinode* spacecraft (Kosugi *et al.*, 2007). The SOT-SP data were calibrated by the standard SP_PREP.PRO routine developed by Lites and Ichimoto (2013) and are available in the SolarSoft package.

SOT-SP obtains Stokes profiles of two magnetically sensitive Fe I lines at 630.15 nm and 630.25 nm. Photospheric vector magnetograms were derived by Stokes inversion based on the assumption of the Milne–Eddington atmosphere (Skumanich and Lites, 1987; Lites *et al.*, 1993). The 180° ambiguity in the vector azimuth was resolved using the minimum-energy algorithm by Metcalf (1994).

The active region NOAA 10930 appeared on the east limb of the Sun on 3 December 2006. Figure 1 (left) shows an example of vector magnetograms on 12 December 2006. The small N-polarity sunspot showed an anti-clockwise rotation and emergence of magnetic flux. The large S-polarity sunspot was well developed. The transverse field vectors were highly sheared near the polarity inversion line (PIL) (Zhang, Li, and Song, 2007; Min and Chae, 2009; Ravindra, Venkatakrishnan, and Tiwari, 2011; Ravindra *et al.*, 2011). The continuum intensity image (right) shows that the penumbral fibrils were parallel to the PIL.

We analyzed the net current, net twist current (NTC), and net shear current (NSC) in the active region separately for the N- and S-polarities. We selected only the pixels whose B_z values were higher than 50 G to avoid noise in the current density computations.

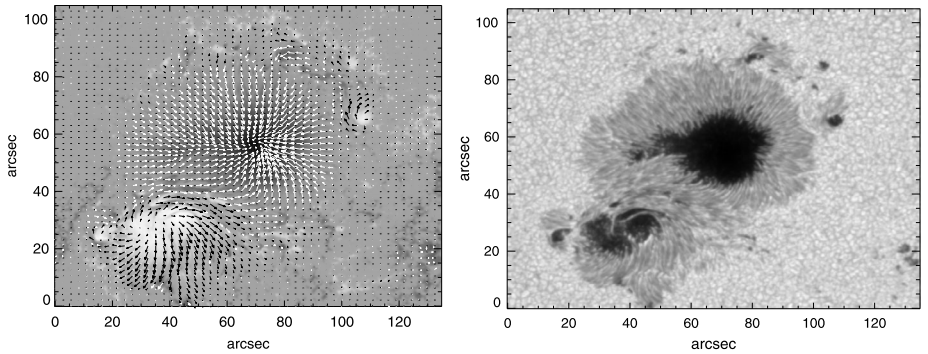

Figure 1 Maps of vector magnetic fields (left) and continuum intensity (right) of AR 10930 at 17:00 UT on 12 December 2006 obtained with *Hinode*/SOT-SP.

4. Results

Figure 2 shows the distributions of vertical current density J_z (left column), shear current density $J_{\rm shear}$ (middle column), and twist current density $J_{\rm twist}$ (right column) on different days during the evolution of the active region. The maps clearly show that the net current originates from the S-polarity region and terminates in the N-polarity region. The twist current density is stronger in the umbrae of both N- and S-polarity regions, while the shear current is weaker in the umbrae. The twist current density follows the net current density and is dominant at two patches of opposite signs in the S- and N-polarity sunspots. These patches increased in strength until 11 December and then decreased.

Figure 3 shows maps of ratios R_1 and R_2 (given by Equations (4) and (5)) and field strength B. The maps indicate that the contributions of R_1 and R_2 are opposite to each other throughout, and both have an alternating band pattern around the umbrae.

Figure 4 shows the evolution of net current, NTC, and NSC integrated over the whole active region. NTC and NSC behaved oppositely from 9 December to 15 December. After 12 December, NTC and NSC changed signs. Since the net current in the S- and N-polarities are equal and opposite at all times, and the net current equals the sum of the twist and shear currents at all times, the sum of NTC and NSC for the whole active region must vanish at all times.

Figure 5 shows the evolution of NTC of the N-polarity (bottom) and S-polarity (top) regions. Initially, the current was weak, until 10 December. Later, it increased linearly in both polarities until the middle of 11 December, and then it started to decrease until the end of 14 December. The behavior of NTC is almost the same in both polarities. The largest value of the twist current is 9.8×10^{12} A in the S-polarity and -9.7×10^{12} A in the N-polarity regions. The negative twist current was dominant in the N-polarity region, and in the S-polarity region the positive twist current was dominant.

Figure 6 shows the evolution of NSC of the N-polarity (top) and S-polarity (bottom) regions. Initially, the current was weak, until 10 December. The shear current was positive and sometimes negative in the N-polarity region. The largest value of the shear current is 3.5×10^{12} A in the N-polarity region, which is smaller than the maximum of the twist current. In the S-polarity region, the maximum of the shear current in its absolute value is -1.6×10^{12} A. The shear current was negative until 14 December and changed its sign after that in the S-polarity region.

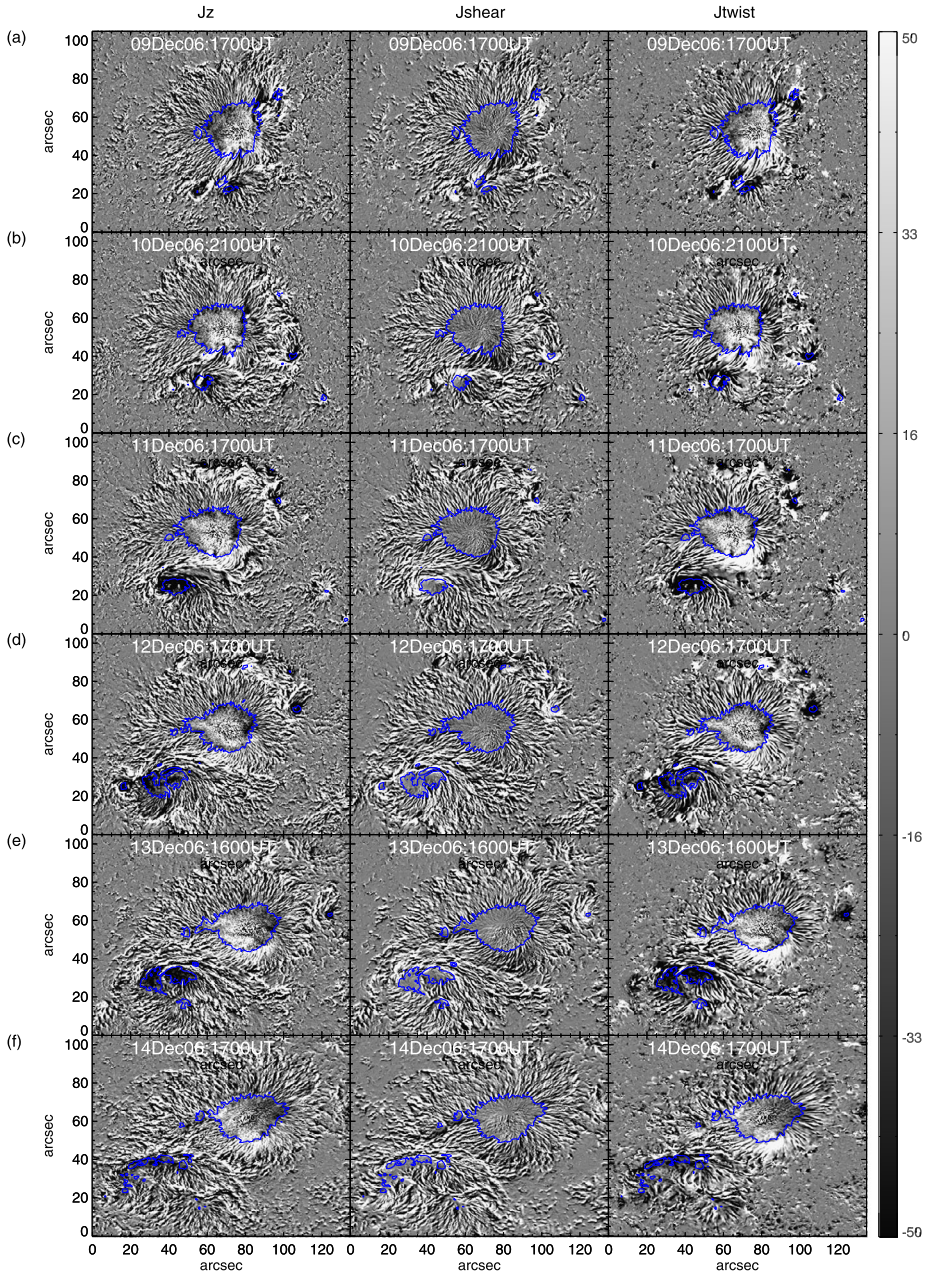

Figure 2 Maps of the distribution of vertical current density (left column), shear current density (middle column), and twist current density (right column) as a function of time. The gray color bar on the right shows the range of current density $\pm$ A m^{-2}. Blue contours represent the sunspot umbrae.

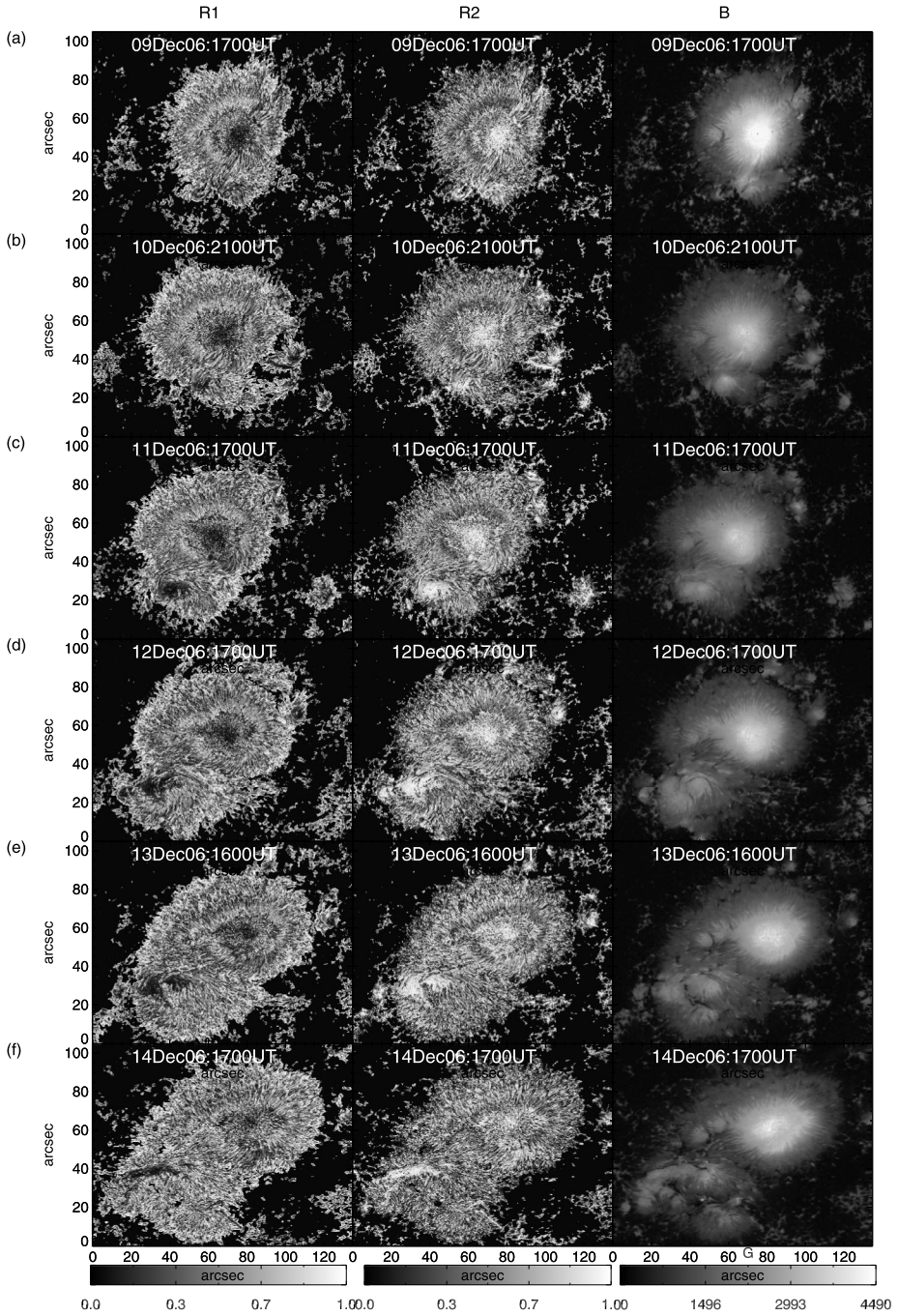

Figure 3 Maps of the ratio between shear current density and net current density (left column), ratio between twist current density and net current density (middle column), and the magnetic field strength (right column) as a function of time. A gray-scale color bar is given below each column.

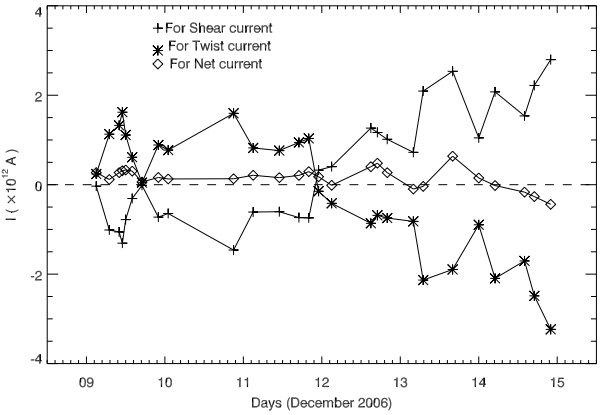

Figure 4 The evolution of net current, NTC, and NSC for the whole AR as a function of time.

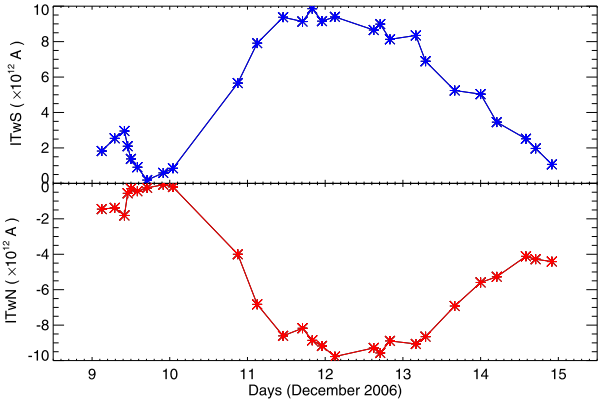

Figure 5 The evolution of NTC in the S-polarity (blue) and N-polarity (red) regions as a function of time.

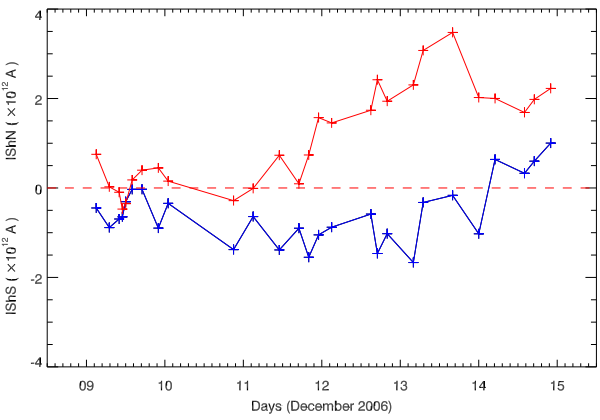

Figure 6 The evolution of NSC in the N-polarity (red) and S-polarity (blue) regions as a function of time.

Figure 7 shows the evolution of the net current (NTC+NSC) in the N-polarity (bottom) and S-polarity (top) regions. Initially, the current was weak, until 10 December. Later, it increased linearly in both polarities until the middle of 11 December, and then it started

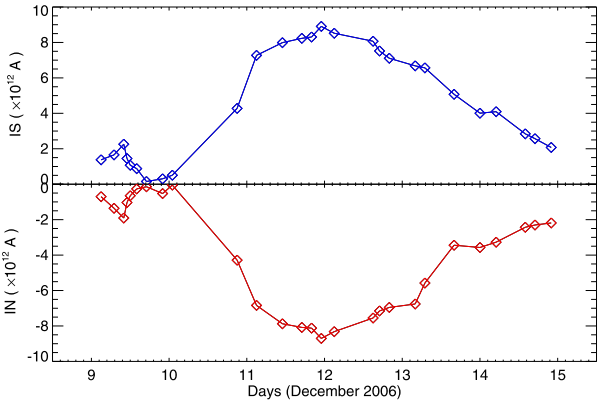

Figure 7 The evolution of net current (NTC+NSC) in the S-polarity (blue) and N-polarity (red) regions as a function of time.

to decrease until the end of 14 December. The behavior of the net current is almost the same in both polarities. The largest value of the net current is 8.9×10^{12} A in the S-polarity region and the maximum of the net current in the absolute value in the N-polarity region is -8.7×10^{12} A. The negative current was dominant in the N-polarity region, while in the S-polarity region the positive current was dominant. This is similar to Figure 2 of Ravindra *et al.* (2011).

Figure 8 shows the evolution of positive (+) and negative (−) components of the twist current ITw in the S-polarity (top) and N-polarity (bottom) regions; ITwN(+), ITwN(−), ITwS(+), and ITwS(−). ITwS(+) increased till 12.5 December and then started to decrease until the end of 14 December. The largest value of ITwS(+) is 3.0×10^{13} A and the smallest value of ITwS(+) is 1.9×10^{13} A. At the same time, ITwS(−) remained almost constant with a value between -2.1×10^{13} A and -1.7×10^{13} A. A similar behavior is also found in the N-polarity region. ITwN(−) increased until 12.3 December and then decreased until the end of 14 December. The maximum of ITwN(−) in the absolute value is -2.1×10^{13} A and the smallest value of ITwN(−) is -1.1×10^{13} A. ITwN(+) remained almost constant with a value between 0.9×10^{13} A and 1.2×10^{13} A.

Figure 9 shows the evolution of positive (+) and negative (−) components of the shear current ISh in the S-polarity (top) and N-polarity (bottom) polarity regions; IShN(+), IShN(−), IShS(+), and IShS(−). Initially, IShS(+) and IShS(−) were weak, until 10 December. Later, IShS(+) increased linearly until the middle of 11 December, and then IShS(+) fluctuated until 14.2 December, while IShS(−) fluctuated before 12.7 December. Then both IShS(+) and ISHS(−) started to decrease until the end of 14 December. The largest values of IShS(+) and IShS(−) are 2.6×10^{13} A and IShS(−) is -2.7×10^{13} A, respectively. IShN(+) and IShN(−) are roughly equal and opposite for all times. The largest values of IShN(+) and IShN(−) are 2.1×10^{13} A and -1.8×10^{13} A, respectively.

Figure 10 shows the evolution of net current, NTC, and NSC for the umbra in the S-polarity (top) and N-polarity (bottom) regions. The largest value of the net current, NTC and NSC are 0.9×10^{12} A, 1.4×10^{12} A, and -0.6×10^{12} A for the umbra in the S-polarity region, while in the N-polarity region, the largest value of the net current, NTC, and NSC are -2.0×10^{12} A, -2.1×10^{12} A, and -0.2×10^{12} A. The shear current was very weak in both umbrae at all times.

Figure 11 shows the evolution of net current, NTC, and NSC for the penumbra in the S-polarity (top) and N-polarity (bottom) regions. Initially, the net current and twist current were weak, until 10 December. Later, both currents increased linearly in both polarities

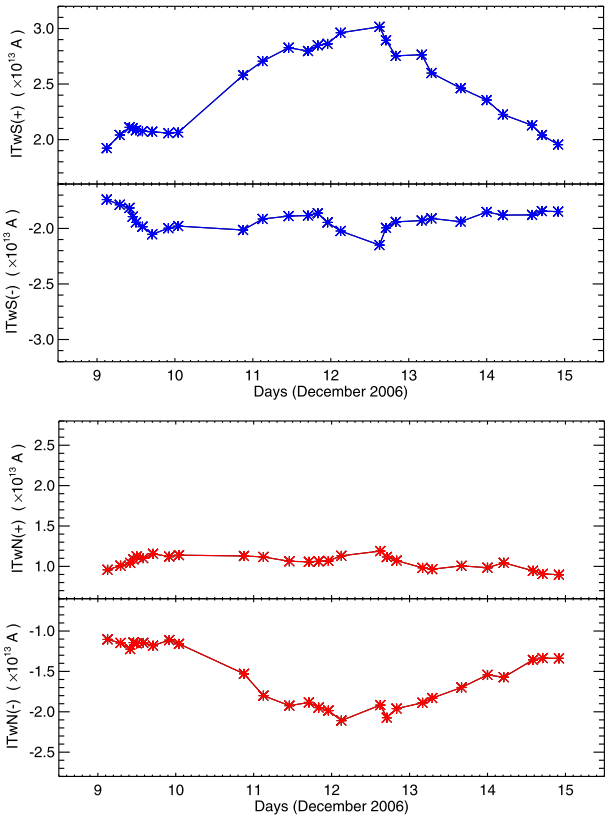

Figure 8 The evolution of NTC in the S-polarity (top) and N-polarity (bottom) regions as a function of time. The top and bottom plots show the evolution of positive and negative currents in the same polarity region.

until the middle of 12 December, and then started to decrease until the end of 14 December. The largest value of the net current, NTC, and NSC are 3.1×10^{12} A, 3.8×10^{12} A, and -0.9×10^{12} A for the penumbra in the S-polarity region, while in the N-polarity region, the largest values of the net current, NTC, and NSC are -3.0×10^{12} A, -3.8×10^{12} A, and 1.7×10^{12} A.

5. Discussion

We calculated the net current in solar active region NOAA 10930 as the sum of the twist and shear currents using a time series of photospheric vector magnetograms of *Hinode*/SOT-SP. This AR was highly eruptive and produced a number of large flares. The distributions of vertical current, shear current, and twist current densities separately evaluated in the N- and S-polarity regions indicate that most of the current originated from the dominant S-polarity region and the opposite current originated from the smaller N-polarity region as in Figure 2.

From the time series of the distribution of current density, we see that the emerging N-polarity rotated in the anti-clockwise direction and the S-polarity did not display any rotation. Currents were distributed as filamentary structures over a major portion of the sunspots except at a few locations in each polarity, where a patchy distribution is seen. The patches grew in strength until 11 December and then started to decrease, whereas the rotation of the N-polarity sunspot became faster from 11 – 13 December, then decreased

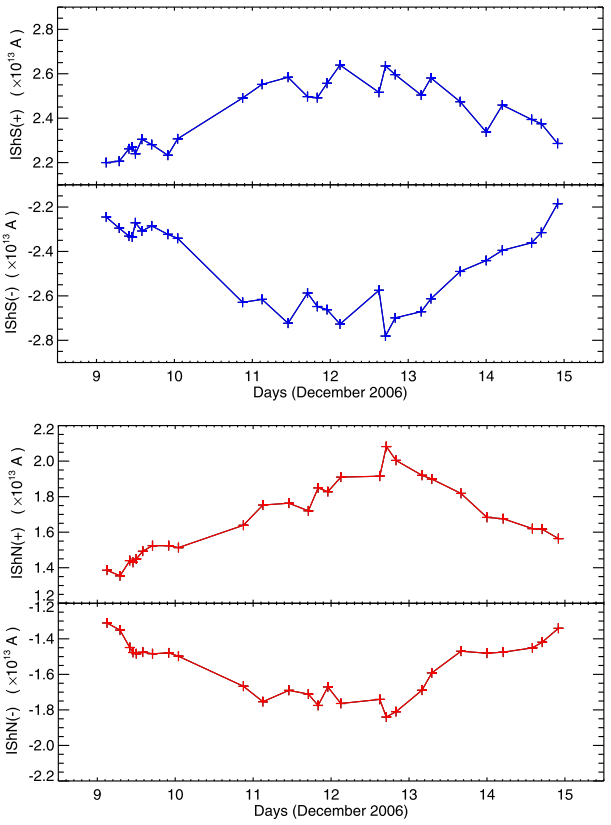

Figure 9 The evolution of NSC in the S-polarity (top) and N-polarity (bottom) regions as a function of time. The top and bottom plots show the evolution of positive and negative currents in the same polarity region.

after the flare (Min and Chae, 2009). The patches of strong current density were located at the footpoints of the emerging flux rope that was identified by Schrijver *et al.* (2008).

The umbrae in the S-polarity region shows mixed signs of current density, while the fibril pattern is present in the penumbra. In the umbra of both polarities, the shear current density was very weak; therefore the twist was dominant in the umbrae region throughout. The evolution of the twist current density follows the net current density. The twist current density was larger than the shear current density throughout the time span of the observation. Thus most of the current was due to the twist. Based on Figure 2, we note that the footpoints of emerging flux were mostly dominated by the twist current.

By examining the maps of ratios R_1 and R_2 (Figure 3), we can compare the contributions of the shear current density and twist current density in the whole active region. R_1 and R_2 are complementary to each other by definition. It is obvious from Figure 3 that R_1 and R_2 have alternating patterns radially outward. From the map of field strength B, we can say that the pattern of low and high shear depends on the radial distribution of the gradient of B. In the umbra, there is a local maximum of B, so that the gradient of B is almost zero. Thus the shear current density is very weak compared with the twist current, and therefore R_2 is very large in the umbra of any sunspot. However, R_2 in the N-polarity umbra is larger than R_2 in the S-polarity umbra. This clearly indicates that the curl $\boldsymbol{b}$ in the N-polarity umbra is much stronger than that in the S-polarity umbra, which is consistent with the fast rotation of the N-polarity sunspot. Zhang (2010) showed the relationship between electric current and individual magnetic fibrils in the same active region for 12 December. He analyzed the

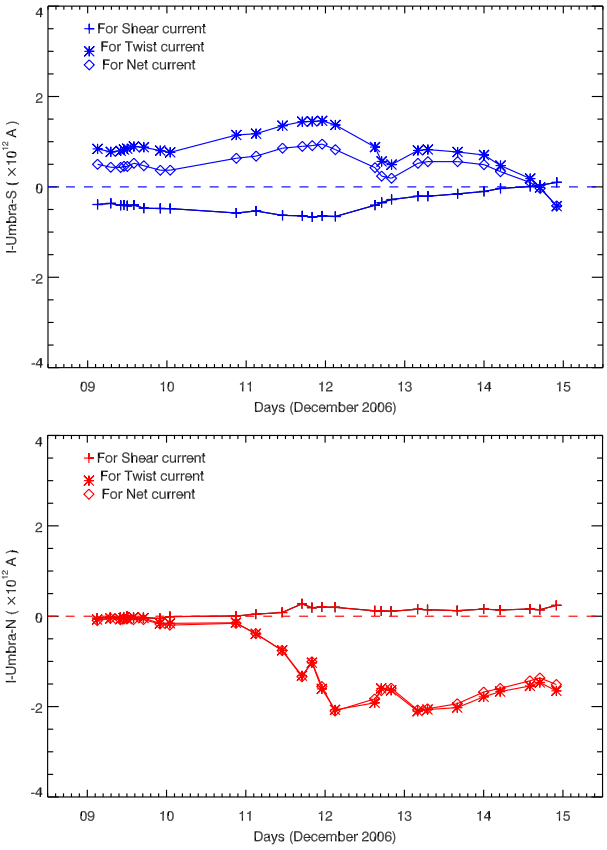

Figure 10 The evolution of net current, NTC, and NSC for the umbra in the S-polarity (top) and N-polarity (bottom) regions as a function of time.

highly sheared magnetic field in the PIL and concluded that the individual magnetic fibrils were dominated by the shear current density caused by the magnetic inhomogeneity while the large-scale magnetic region was dominated by the twist current. Our results suggest that mostly twist current was dominant in the umbrae and penumbrae. The shear current density and twist current density were dominant in alternate bands around the umbrae for the rest of the active region throughout. However, the modulation amplitude of the bands was somewhat reduced after the X3.4 class flare that occurred on 13 December 2006 at 02:14 UT.

Thus far, we have discussed the local distribution of shear and twist current densities. We now discuss the global current that is the surface integral of current density.

The net twist currents (NTC) in the N- and S-polarity regions behaved exactly opposite to each other during their evolution. This finding clearly indicates that the twist current flew from one polarity to the corona and returned to the photosphere in the other polarity. In a study of the same active region, Ravindra *et al.* (2011) showed that the symmetrical evolution of the net current was due to the evolution of the shear in the PIL, but it was not so straightforward to understand the evolution of the twist current as seen in our results. Our results indicate that the twist current gradually decreased after the onset of the X3.4 class flare of 13 December 2006.

Furthermore, it is now acknowledged that the sign of helicity is maintained in different layers of the solar atmosphere (Tiwari, Venkatakrishnan, and Sankarasubramanian, 2010).

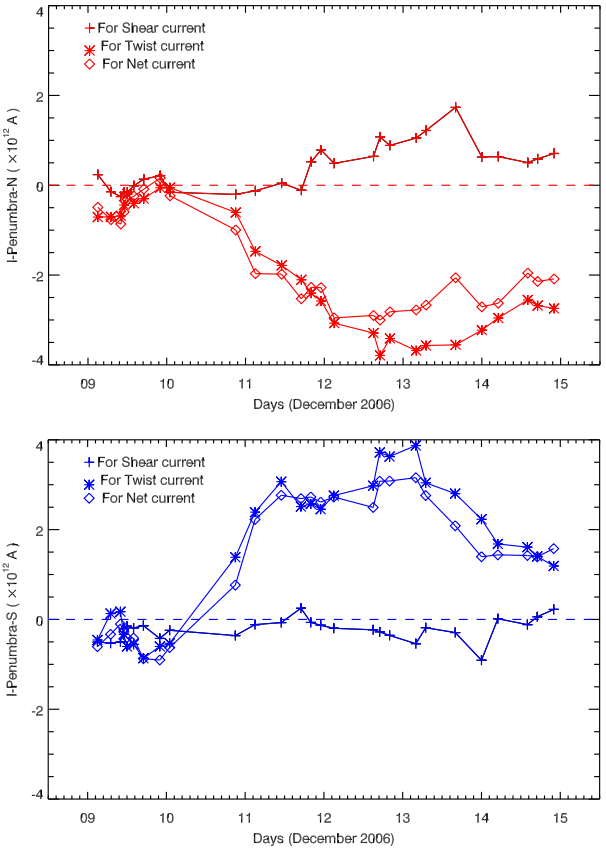

Figure 11 The evolution of net current, NTC, and NSC for the penumbra in the S-polarity (top) and N-polarity (bottom) regions as a function of time.

This indicates that there is a coupling between the helicity in the photosphere, chromosphere, and corona. This coupling can be studied in more detail by monitoring the evolution of twist current in different layers of the solar atmosphere.

Acknowledgements We thank the referee for useful comments and suggestion that improved the paper. *Hinode* is a Japanese mission developed and launched by ISAS/JAXA, with NAOJ as domestic partner and NASA and STFC (UK) as international partners. It is operated by these agencies in co-operation with ESA and the NSC (Norway).

References

Abramenko, V.I., Gopasiuk, S.I., Ogir', M.B.: 1991, *Solar Phys.* **134**, 287.
Chen, J.M., Zhang, H.Q.: 1992, *Acta Astrophys. Sin.* **12**, 82.
Ding, Y.J., Hong, Q.F., Hagyard, M.J., Deloach, A.C., Liu, X.P.: 1987, *Solar Phys.* **109**, 307.
Hofmann, A., Kalman, B.: 1991, *Astron. Astrophys.* **241**, 203.
Ichimoto, K., Lites, B., Elmore, D., Suematsu, Y., Tsuneta, S., Katsukawa, Y., 2008, *Solar Phys.* **249**, 233.
Kosugi, T., Matsuzaki, K., Sakao, T., Shimizu, T., Sone, Y., Tachikawa, S., 2007, *Solar Phys.* **243**, 3.
Krall, K.R., Smith, J.B., Jr., Hagyard, M.J., West, E.A., Cummings, N.P.: 1982, *Solar Phys.* **79**, 59.

Leka, K.D., Barnes, G.: 2003, *Astrophys. J.* **595**, 1296.
Leka, K.D., Canfield, R.C., McClymont, A.N., van Driel-Gesztelyi, L.: 1996, *Astrophys. J.* **462**, 547.
Lin, Y., Gaizauskas, V.: 1987, *Solar Phys.* **109**, 81.
Lites, B.W., Ichimoto, K.: 2013, *Solar Phys.* **283**, 601.
Lites, B.W., Elmore, D.F., Seagraves, P., Skumanich, A.P.: 1993, *Astrophys. J.* **418**.
Metcalf, T.R.: 1994, *Solar Phys.* **155**, 235.
Min, S., Chae, J.: 2009, *Solar Phys.* **258**, 203.
Moreton, G.E., Severny, A.B.: 1968, *Solar Phys.* **3**, 282.
Parker, E.N.: 1979, *Cosmical Magnetic Fields: Their Origin and Their Activity*, Clarendon Press, New York, 858.
Parker, E.N.: 1996, *Astrophys. J.* **471**, 485.
Ravindra, B., Venkatakrishnan, P., Tiwari, S.K.: 2011, In: Satake, K. (ed.), *Advances in Geosciences, Solar Terrestrial (ST)* **27**, World Scientific, Singapore, 153.
Ravindra, B., Venkatakrishnan, P., Tiwari, S.K., Bhattacharyya, R.: 2011, *Astrophys. J.* **740**, 19.
Schrijver, C.J., De Rosa, M.L., Metcalf, T., Barnes, G., Lites, B., Tarbell, T., 2008, *Astrophys. J.* **675**, 1637.
Shimizu, T., Nagata, S., Tsuneta, S., Tarbell, T., Edwards, C., Shine, R., 2008, *Solar Phys.* **249**, 221.
Skumanich, A., Lites, B.W.: 1987, *Astrophys. J.* **322**, 473.
Suematsu, Y., Tsuneta, S., Ichimoto, K., Shimizu, T., Otsubo, M., Katsukawa, Y., 2008, *Solar Phys.* **249**, 197.
Tiwari, S.K., Venkatakrishnan, P., Sankarasubramanian, K.: 2010, In: Hasan, S.S., Rutten, R.J. (eds.) *Magnetic Coupling Between the Interior and Atmosphere of the Sun*, Springer, Berlin, 443.
Tsuneta, S., Ichimoto, K., Katsukawa, Y., Nagata, S., Otsubo, M., Shimizu, T., 2008, *Solar Phys.* **249**, 167.
Wang, J., Shi, Z., Wang, H., Lue, Y.: 1996, *Astrophys. J.* **456**, 861.
Zhang, H.: 1995, *Astron. Astrophys.* **304**, 541.
Zhang, H.: 2001, *Astrophys. J. Lett.* **557**, L71.
Zhang, H.: 2010, *Astrophys. J.* **716**, 1493.
Zhang, J., Li, L., Song, Q.: 2007, *Astrophys. J. Lett.* **662**, L35.